IMAGING OF THE FLAME SOOT FORMATION BY HRTEM

J.N. Rouzaud, Laboratoire de Géologie - Ecole Normale Supérieure, UMR CNRS 8538, Paris – France
M. Alfè, B. Apicella, R. Barbella, A. Tregrossi, A. Ciajolo, Istituto di Ricerche sulla Combustione - C.N.R., P.le Tecchio, 80, Naples – ITALY
M. Pawlyta, S. Duber, University of Silesia, Faculty of Earth Sciences, Sosnowiec - POLAND

Introduction

The study of the organization of the graphitic layers of soot at a nanostructural scale (i.e. dimension and orientation of the graphitic layers) is driven by their role in the soot reactivity toward oxidation and in the optical properties. Structural differences of soot reflecting in different reactivity and optical properties have been found in dependence on fuel and synthesis/combustion conditions by means of Transmission Electron Microscopy (TEM) (Vander Wal 2003, Rouzaud 2004) and UV-Visible spectroscopy (Alfè, 2007).
A structural description of early and mature soot sampled from aliphatic and aromatic-fuel premixed flames, burning in fuel rich condition, has been performed by means of High Resolution Transmission Electron Microscopy (HRTEM). Different nanostructures have been found to develop in the soot depending on the fuels characteristics. HRTEM image analysis was carried out to achieve quantitative information about the soot organization. The soot formation process has been also investigated by UV-visible spectroscopy and an attempt to correlate soot structure (for instance the length of the graphitic layers, size of the coherent domains made of stacked layers) with UV-Visible spectroscopic characteristics, H/C molar ratio and oxidation reactivity has been also made.

Experimental

Flame-formed soot was isokinetically collected in a premixed laminar ethylene/O_2 flame (C/O= 1, maximum flame temperature 1670 K) and in a benzene/O_2/N_2 (77%) flame (C/O = 0.8, maximum flame temperature 1809 K) produced on a commercial McKenna burner (McKenna Products Inc., USA) at atmospheric pressure. A stainless-steel water-cooled probe vertically inserted in flame was used to sample combustion products along the flame axis. Solid and tarry material (total particulate) collected on the probe wall, on a Teflon filter and in an ice-cooled trap placed along the sampling line, were extracted by dichloromethane (DCM) to separate the DCM soluble material (condensable species) from the insoluble solid carbonaceous material (soot). More detail on the sampling and separation procedure are given elsewhere (Ciajolo 1994).
H/C atomic ratio of soot was measured by a Perkin-Elmer 2400 CHNSO elemental analyzer.
Thermogravimetric analyses (TGA) were performed on a Perkin-Elmer Pyris 1 TGA (Thermogravimetric Analyzer) by heating the dry soot from 30°C up to 850°C at a rate of 10°Cmin^{-1} and under air flow (30 ml min^{-1}).
UV-Visible spectra of soot, suspended in N-methylpyrrolidinone (NMP), were measured on an HP 84523 Diode Array spectrophotometer in the 200-800 nm wavelength region by using 1 cm path-length quartz cuvette.
Transmission Electron Microscopy (TEM) analyses were performed on a JEOL 2011 electron microscope operating at 200kV (resolution in the lattice fringe mode 0.144 nm).
The multiscale organization was analysed at 50,000X magnification. In order to determine the average primary particle diameter, each individual particle shape was approximated by a circle with area equal to the area of the particle in the image. About 2000 measurements were performed for each soot sample, and average value and standard deviation of primary particles diameter (dp) were determined. The number of classes was defined as k = 1+3.3ln(N), where N is a number of measured particles; minimal number of class including minimum 68% of obtained results and their range (Z) were determined.
The high-resolution images were obtained in the 002 lattice fringe mode at 400,000X magnification. Each fringe represents the profile of a polyaromatic layer, i.e. of a graphene plane. A software of HRTEM image analysis was used to obtain quantitative structural information. This lab-made software was especially developed to characterize nanostructured carbons as soot from skelettonized images, i.e. from processed binary images where the fringes are one-pixel width (Shim 2000, Galvez 2002, Rouzaud 2002). Pairs of fringes were here considered as stacked layers to form coherent domains (i.e. Basic Structural Units, BSU), when their angle is smaller than15° and their inter-layers spacing narrower than 0.6 nm. The software allows to determine the proportion of non stacked layers (nsl), the number N of stacked layers in a BSU, the diameter La and the height Lc of these BSU.

Results and Discussion

Figure 1 shows TEM images of young soot sampled in the soot inception region of benzene (7 mm of flame height, left side of Figure 1) and ethylene (8 mm of flame height, right side of Figure 1) flames and in the zone where soot reaches its maximum concentration, here named mature soot (16 mm for benzene soot and 14 mm for ethylene soot).
The texture of soot (upper part of Figure 1) consists of spherical primary particles, with a narrow size distribution, connected in loose, open aggregates.

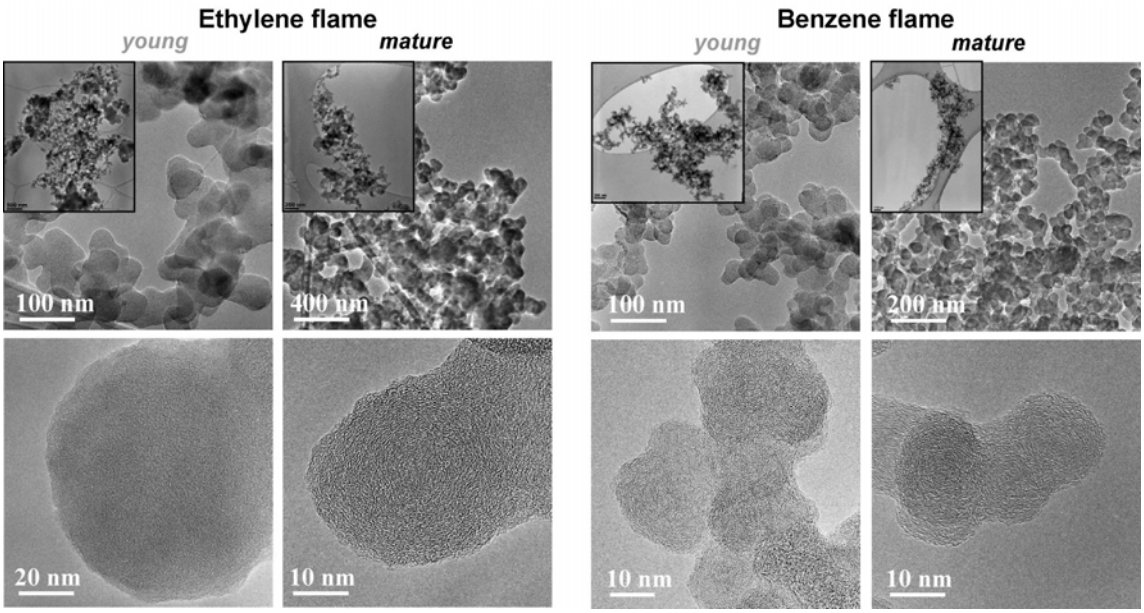

Figure 1. TEM and HRTEM of benzene (left) and ethylene soot (right).

It is worth to note that both young and mature soot present a certain degree of heterogeneity: big coalesced amorphous-like particles are visible in the TEM image of young ethylene soot (Figure 1, upper right side, inset) whereas remnants of amorphous-like carbon, attached to the primary particles of the aggregates, are present in mature ethylene soot and in the benzene soot (both young and mature). Such amorphous-like carbon particles are present in a very smaller amount in the soot from the benzene flame than in the soot from ethylene flame and probably correspond to randomly deposited PAH-like structures, having different sizes, which are the elemental bricks of the soot nanoparticles formation (Bockhorn, 1994). The initial concentric association of these polyaromatic structures gives 'seeds' of further onion-like nanoparticles.
Textural parameters of the investigated samples, measured by TEM image analysis, are gathered in Table 1. N corresponds to number of measured particles, dp to the primary particles diameter and Z is the range that includes minimum 68% of obtained results.

Table 1. Structural parameters inferred by TEM image analysis, nm.

	benzene		**ethylene**	
	young soot	*mature soot*	*young soot*	*mature soot*
N	1802	2597	2341	2094
dp, nm	38 ± 13	20 ± 5	74 ± 39	41 ± 9
Z, nm	25 - 46	15 - 25	21 - 86	28 - 47

Histograms of particles diameter obtained by image analysis are reported in Figure 2.
The investigated samples are significantly different in their primary particle size. Both young and mature soot derived from benzene flame exhibit smaller primary particles diameter than soot derived from ethylene flame. It is also visible that young soot (derived from ethylene as well as benzene flame) consists of larger primary particles than mature soot. Histograms of particle extent obtained for both ethylene and benzene young soot are non-symmetrical. It is clearly evident that besides the most frequently occurring particles (dp between about 30 to 100 nm for ethylene; dp between about 25 to 50 nm for benzene), considerably larger primary particles (big

coalesced amorphous-like particles) appear (dp nearly 200 nm for ethylene and 100 nm for benzene). Histograms of particle extent obtained for mature soot are symmetrical and do not include coalesced amorphous-like particles.

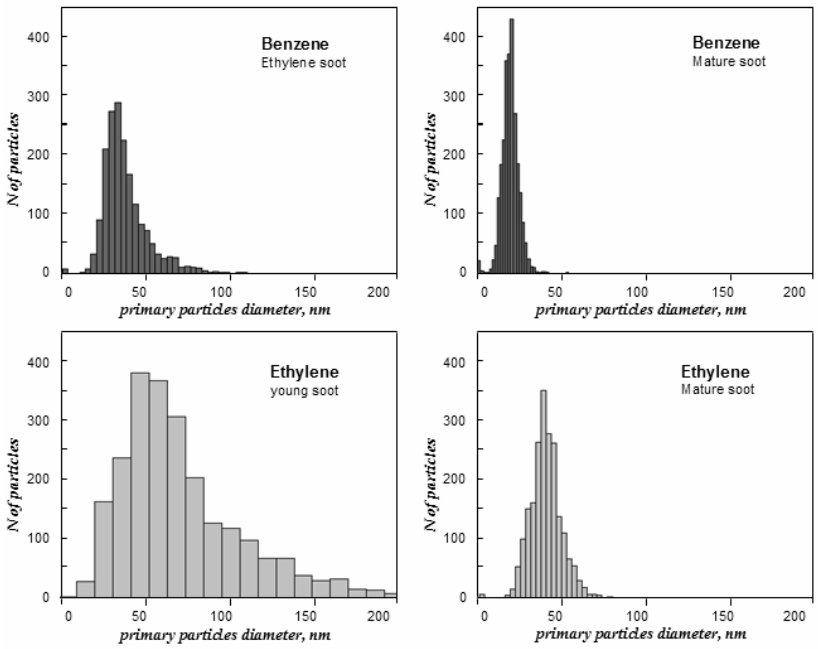

Figure 2. Histograms of primary particles diameters, nm.

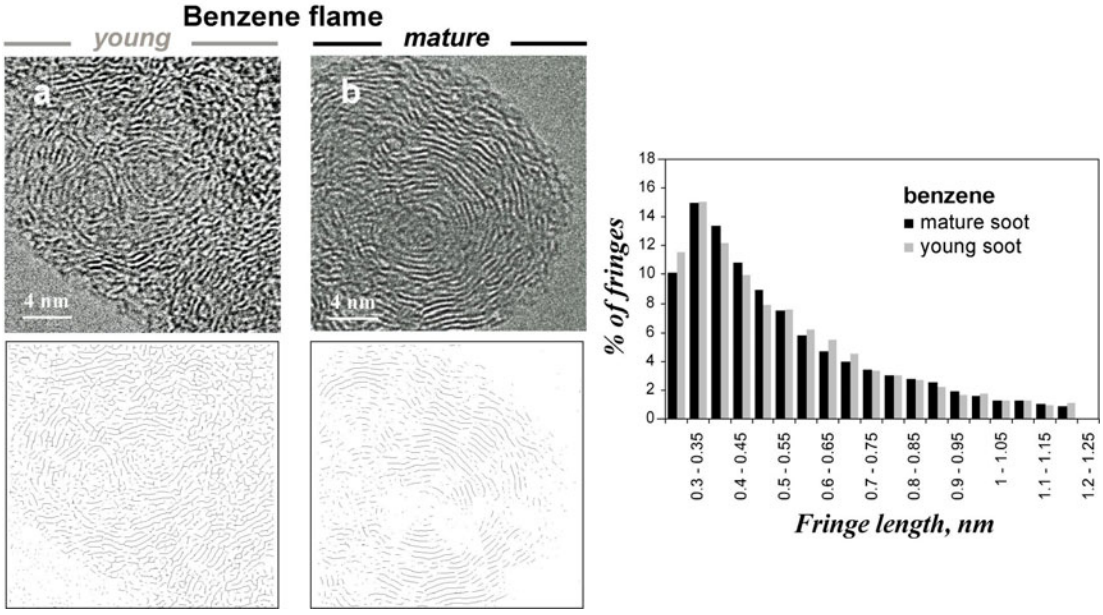

Figure 3. Raw HRTEM images (on the top) and corresponding skeletons below of young benzene soot (left), mature benzene soot (right) and relative histograms of fringe length.

The HR-TEM (lower part of Figure 1 and Figures 3-4) shows different nanoscale organization inside the primary particles of benzene and ethylene soot.
Both young and mature soot derived from benzene flame (Figure 1, lower part) exhibit extended graphene layers with a small radius of curvature. This arrangement gives rise to a more extended surface area with respect to the ethylene soot.

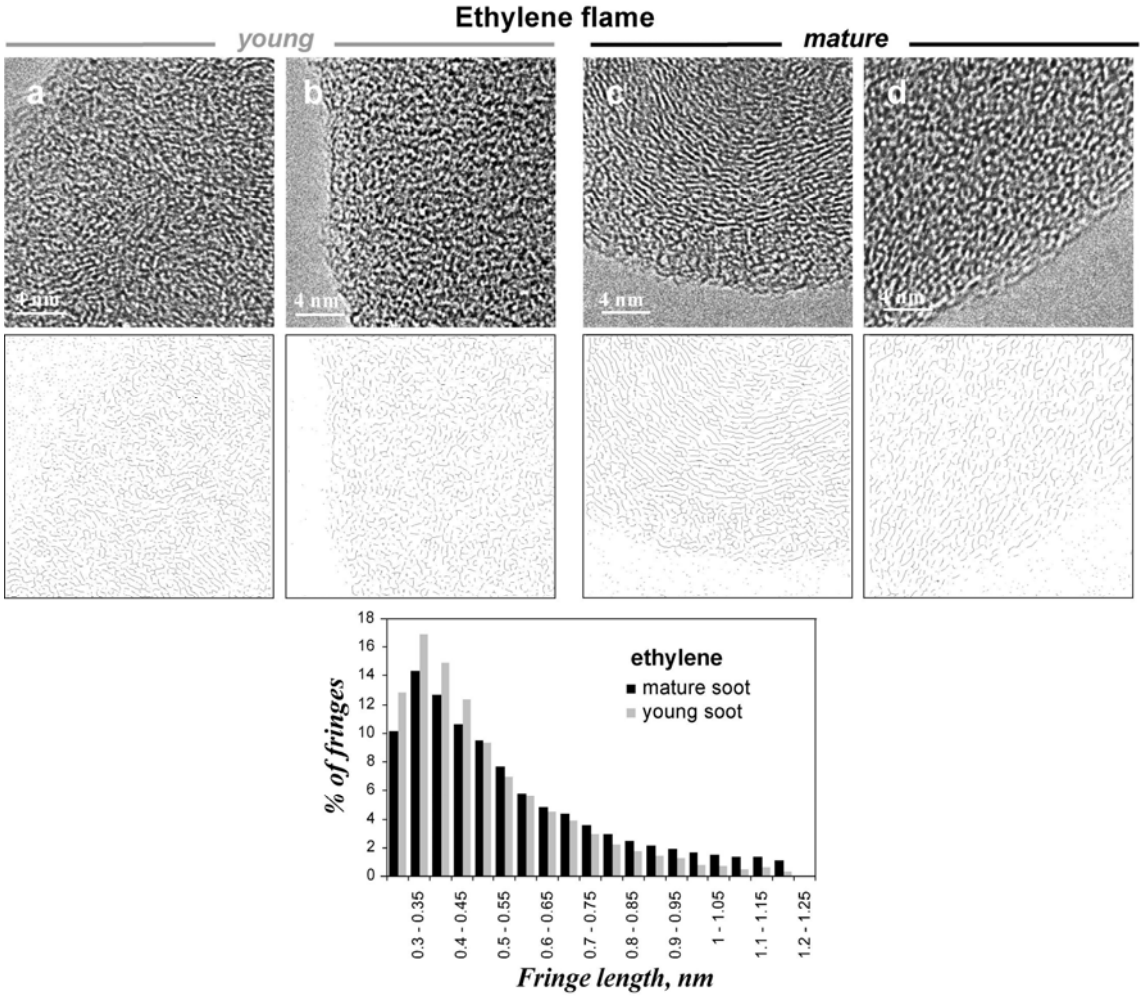

Figure 4. Raw HRTEM images (on the top) and corresponding skeletons below of young ethylene soot (left), mature ethylene soot (right) and relative histograms of fringe length.

The seeds of onion-like structures, already visible in the young benzene soot (Figure 3a), reach well formed concentric shell nanostructures in the mature soot, with diameter from 4 to 10 nm within the best structured areas (Figure 3b). Most onion-like structures form more or less branched aggregates (Figure 1); a central quasi-amorphous 1-2 nanometer core is often observed in the benzene mature soot particles (Figure 3b), as already described by Ishiguro et al, 1997 for diesel soot particles.

By contrast, young ethylene soot appears as a disordered carbon (Figures 4a-b). The concentric organization of the stacked graphitic layers arises at the end of soot formation process extending, in the best structured areas, throughout each primary particles of mature soot (Figure 4c). Remnants of amorphous carbon are discernible (Figure 4d) even if such amorphous content is present in a minor amount with respect the young soot from the ethylene flame (Figure 1).

The skeleton images reported in Figure 3 (benzene soot) and in Figure 4 (ethylene soot) display the regions of interest of the primary particles and the profile of the graphene planes. Table 2 summarizes the structural parameters obtained by image analysis of the skeletonized images that allows to obtain at quantitative measure of the qualitative observation inferred by the HR-TEM images. L corresponds to the mean fringe length and has been evaluated by considering all the fringes larger than the size of 1 aromatic ring ($L > 0.25$ nm) and all the fringes larger than the size of 2 fused aromatic rings ($L > 0.49$ nm), La and Lc correspond to the diameter and to the height of the coherent domains, i.e. of the BSU, formed by N stacked layers with an interlayer spacing of d. The BSU structural parameters reported in Table 2 represent the mean values evaluated on 15-20 images representative of the best structured areas.

The BSU structural parameters L, La, Lc, N of the young benzene soot are higher than those of young ethylene soot indicating a better organization with respect to the ethylene soot. It is also noteworthy that the BSU parameters of young and mature benzene soot are quite similar. By contrast, the BSU structural parameters of ethylene soot indicate an increase of the structural order from young to mature soot.

Table 2. Structural parameters inferred by HR-TEM image analysis, Å.

	benzene		ethylene	
	young soot	*mature soot*	*young soot*	*mature soot*
L (>2.5, θ = 40%)	5.5	6.0	4.9	6.0
L (>4.9, θ = 40%)	8.0	8.7	7.2	8.5
La (>2.5, θ = 15%)	3.6	4.7	2.9	4.1
d (>2.5, θ = 15%)	3.8	3.8	3.8	3.8
N (>2.5, θ = 15%)	2.6	2.9	2.4	2.7
Lc (>2.5, θ = 15%)	5.9	7.0	5.1	6.5

The histograms of the fringe lengths L for each of the four soot analysed, evaluated admitting a 40% of fringe tortuosity, are reported in Figures 3-4 (benzene and ethylene soot, respectively). The fringe length distribution for the young benzene soot is comparable to that of the mature one, whereas a shift toward higher values can be observed passing from young to mature ethylene soot. It is worth to note that the length distribution of the mature benzene soot is the same of the mature ethylene soot in spite of the observed differences in the curvature of graphene segments visible in the HRTEM reported in the Figures 3 –4.

The better organization of young benzene soot can be attributed to the flame environment in which benzene soot is formed that is very rich of aromatic radicals/species and relatively poor in unsaturated light hydrocarbons. The aromatic species act as building bricks of soot particles which can coalesce and coagulate forming relatively much ordered aromatic structures. The poorness in light unsaturated hydrocarbons, importantly involved in the formation of the first aromatic ring and in the following surface growth processes in aliphatic fuel flames, avoid the "intrusion" of these species in the first seeds of soot, limiting the disordering of the young benzene soot structure.

The interlayer spacing, d, typical of poorly ordered carbons (0.38 nm in comparison with the 0.3354 nm graphite value) is the same for both benzene and ethylene soot.

In few works, such large structural changes have been observed, in dependence on fuel and synthesis conditions (Vander Wal 2003, Rouzaud 2004) and a correlation between soot nanostructure and soot reactivity toward oxidation has been proposed (Vander Wal 2003) assuming that the reactivity toward oxidative attack depends on two main factors:

i - accessibility of carbon in edge sites that are more reactive than the basal plane carbon atoms.

ii - weakening of C-C bonds for effect of curvature due to five-member rings (driving to an increase of sp^3 character, like in fulleroid structures (Ebbesen 1997, Dresselhaus 1996).

Vander Wal pointed out that, provided that the length of the graphitic layers are the same (i.e. the accessibility of the carbon edge sites), the more the curvature of the soot is enhanced, the faster the reactivity toward oxidation. Similar observations were made by Rouzaud et al, 2004 on a series of carbon blacks, nanostructurally similar to the here studied soot.

In order to evaluate the effect of soot structure on the oxidation rate, thermogravimetric analyses in oxidative environment of soot have been performed in this work.

The thermogravimetric (TG) curves of the ethylene and benzene soot, reported in the Figure 5, exhibit the main weight loss in the 600-675°C temperature range. The temperature corresponding to the maximum weight loss increases moving from young soot to mature soot for both benzene and ethylene soot testifying the increase of soot resistance to oxidation during the formation process. This trend is more easily discernible on the derivative curves (DTG) also reported in Figure 5.

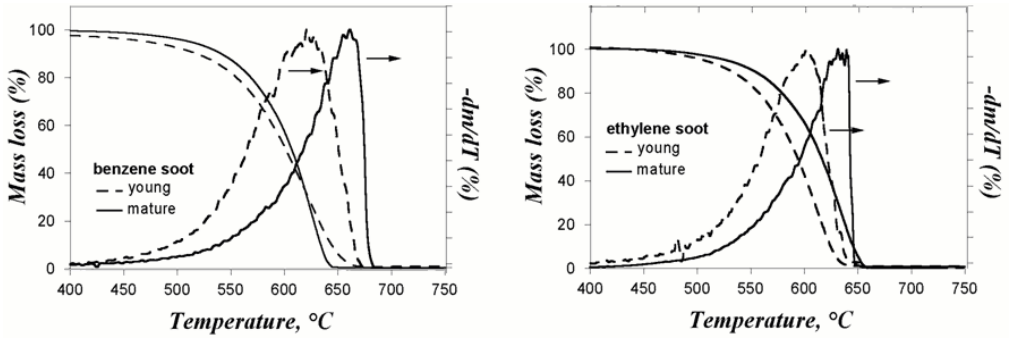

Figure 5. TG and DTG curves (10°Cmin^{-1}) under air (30 ml min^{-1}) corresponding to benzene and ethylene soot.

The higher resistance toward oxidation of mature soot can be associated to the increase of the layer plane size, L, from young to mature soot (Table 2), i.e. to the minor number of carbon edge sites accessible. Benzene soot is more resistant to oxidation with respect to the ethylene soot (Figure 5) even though benzene soot presents a higher curvature (Figures 2-3). For the young soot, the lower oxidation reactivity of benzene soot is related to the fact that the graphene layers are longer than those measured in the ethylene soot (Table 2) causing the exposition of a low number of edge site carbon atoms to oxidation. For the mature soot, however, this explanation fails since the fringe mean length L of ethylene and benzene soot are almost equal. The lower reactivity of benzene soot can be then interpreted in light of the H/C atomic ratio data reported in Figure 6.

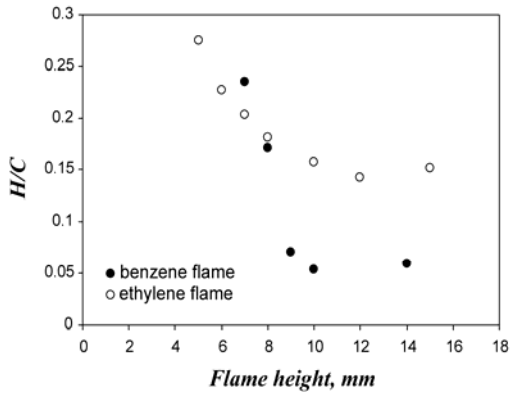

Figure 6. H/C atomic ratio of benzene and ethylene soot

Benzene and ethylene soot show a similar H/C in the early stage of soot formation, but in the soot maturation process the benzene soot reaches a much lower H/C, typical of materials highly resistant to oxidation like carbon black (H/C=0.035 and maximum DTG temperature 710°C as measured in this work). The lower H/C, can be associated to a lower number of active C-H sites available for oxidation attack that justify the higher oxidation resistance of mature benzene soot in spite of the above mentioned larger curvature and similar L dimension with respect to the ethylene soot.

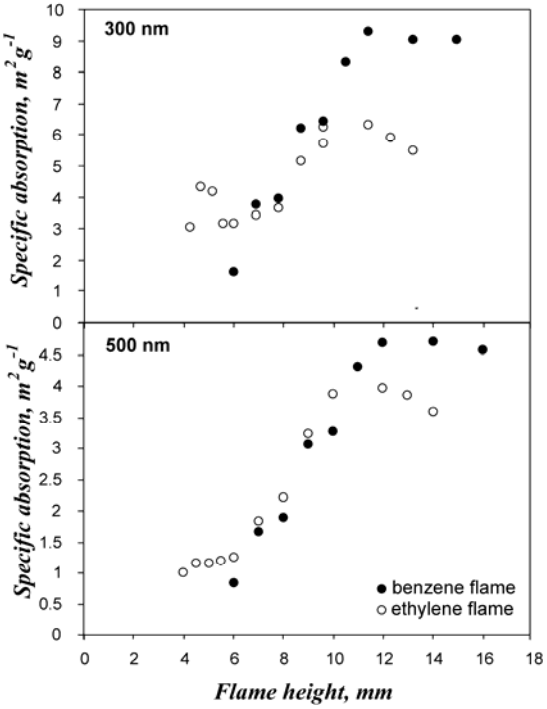

Figure 7. Specific soot absorption of benzene and ethylene soot suspended/dissolved in NMP.

Additional insights in the soot structure are provided by UV-Visible spectroscopy in terms of absorption coefficients and spectral shapes.
The UV-Visible spectra were measured on soot suspended in NMP by means of ultrasonic agitation. Since soot suspensions are complex mixtures of unknown molecular weight, the absorption coefficients have been evaluated on mass basis (m^2/g).
The specific absorption of soot in the UV (300 nm) and in the visible (500 nm), reported in Figure 7, increases along the benzene and ethylene flames reaching higher absorption values at the end of the benzene flame. This corresponds to a higher structural parameter Lc (Table 2), indicative of a higher number of stacked layers in the case of benzene mature soot, that is known to affect the optical properties (Papoular 1996, Duley, 1998, Schnaiter 1998, Jager 1999, Michel 1999).
The Visible/UV absorption ratio of benzene and ethylene soot, reported as a function of the flame height in Figure 8, is also representative of the structural changes occurring in the soot maturation process.

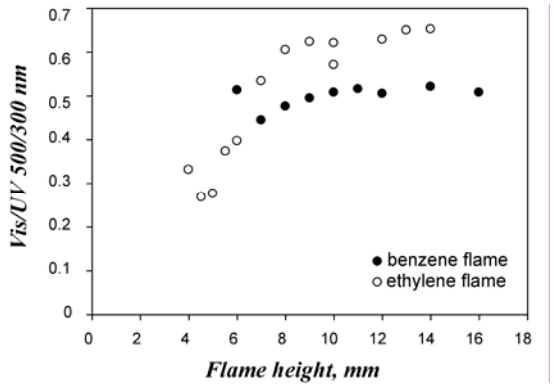

Figure 8. UV-Visible ratio (500/300 nm) of benzene and ethylene soot suspended/dissolved in NMP.

For the ethylene soot, the progressive increase of Visible/UV ratio testifies the occurrence of a structural variation in terms of increase of aromatic island, whereas the Visible/UV ratio of benzene soot remains quite constant along the flame consistently with the constancy of the BSU structural parameters of benzene soot above mentioned (Table 2).

Conclusions

Soot sampled in fuel-rich premixed laminar flames burning aromatic (benzene) and aliphatic (ethylene) fuels in the zone of young soot (soot inception) and in the zone of mature soot (end of flame) has been analyzed in terms of multiscale organization (HRTEM images), including structure and nanostructure, and optical and chemical properties (oxidation reactivity, H/C atomic ratio, UV-Visible spectroscopy).
The multiscale organization of flame formed soot was found related to sensitivity to oxidative attack and to H/C and UV-Visible absorption properties of soot.
Overall, in the benzene soot, layer planes possessing a small radius of curvature forming the seeds of onion-like nanostructure were already visible in the young benzene soot. In the mature benzene soot, well formed onion-like particles (diameter 4-10 nm) were detected. Young ethylene soot appears as a disordered carbon and during soot formation the occurrence and the organization of the graphitic layers arise, responsible for the development of the onion-like nanostructure.
Both ethylene and benzene soot exhibit higher resistance toward oxidation in the maturation process related to the increase of the fringe length and decrease of H/C ratio. Young and mature benzene soot appeared more resistant to oxidation with respect to the ethylene soot. This trend, despite that the length of the graphene layers is the same for the mature benzene and ethylene soot, is related to the much higher H/C atomic ratio of ethylene mature soot, that allows it to offer a larger number of active sites for oxidation attack.
UV-visible absorption coefficients of benzene soot steeply increase along the flame axis reaching at the end of flame values higher than in the ethylene soot. The different spectral features and chemical properties of the benzene soot appear to be related to a different internal structure of primary particles which in turn derives from a different soot inception mechanism.

Acknowledgements

This work has been partially supported by Centro Regionale di Competenza - AMRA, Naples – ITALY and by CNR-CNRS 2006 convention.

References

Alfe`, M., Apicella, B., Barbella, R., Tregrossi, A., Ciajolo, A. 2007. Similarities and dissimilarities in n-hexane and benzene sooting premixed flames. *Proceedings of the 31st Symposium on Combustion* 1:585-591.

Bockhorn, H. 1994. Soot Formation in Combustion. Mechanisms and models. *Chemical Physics 59.* Springer-Verlag.

Ciajolo, A., Barbella, R., D'Anna, A. 1994. PAH and high molecular weight species formed in a premixed methane flame. *Combust. Sci. Technol.* 100:271-278.

Dresselhaus, M.S., Dresselhaus, G., Elkund, P.C. 1996. *Science of Fullerenes and Carbon Nanotubes,* Academic Press Inc.

Duley, W. W., Seahra, S. 1998. Graphite, polycyclic aromatic hydrocarbons, and the 217.5nm extinction feature. *ApJ*, 507:874-888.

Ebbesen, T.W., (Editor) 1997. *Carbon Nanotubes, Preparation and Properties*, CRC Press Inc., 1997.

Galvez, A., Herlin-Boime, M., Reynaud, C., Clinard C., Rouzaud, J-N. 2002. Carbon nanoparticles from laser pyrolysis. *Carbon* 40:2775-2789.

Ishiguro, T., Takatori, Y. and Akihama, K. 1997 Microstructure of Diesel soot particles probed by electron microscopy: First observation of inner core and outer shell. *Combust. Flame*, 108: 231-234.

Jager, C., Henning, Th., Schlogl, R., Spillecke, O. 1999. Spectral properties of carbon black. *Journal of Non-Crystalline Solids* 258:161-179.

Michel, B., Henning, Th., Jager, C., Kreibig, U. 1999. Optical extinction by spherical carbonaceous particles. *Carbon* 37:391–400.

Papoular, R., Conrad, J., Guillois, O., Nenner, I., Reynaud, C., Rouzaud, J-N. 1996. A comparison of solid-state carbonaceous models of cosmic dust. *A&A* 315:222-236.

Rouzaud, J.N., Duber, S., Pawlyta, M., Cacciaguerra, T., Clinard, C. 2004. Relationships multiscale organization – properties. *International Conference Carbon Providence*, Rhode Island, USA.

Rouzaud, J-N, Clinard, C. 2002. Quantitative high-resolution transmission electron microscopy: a promising tool for carbon materials characterization. *Fuel Proc. Tech.* 77-78:229-235.

Schnaiter, M., Mutschke, H., Dorschner, J., Henning, Th., Salama, F. 1998. Matrix-isolated nano-sized carbon grains as an analog for the 217.5 nanometer feature carrier. *ApJ* 498:486-496.

Shim, H-S., Hurt, R., Yang, N. 2000. A methodology for analysis of 002 lattice fringe images and its application to combustion-derived carbons. *Carbon* 38:29-45.

Vander Wal, R.L., Tomasek, A.J. 2003. Soot oxidation: dependence upon initial nanostructure. *Combust. Flame* 134:1-9.